Trop J Nat Prod Res, June 2024; 8(6): 7590 - 7602 **ISSN 2616-0684 (Print)**
ISSN 2616-0692 (Electronic)

Tropical Journal of Natural Product Research

Available online at https://www.tjnpr.org

Original Research Article

Antibacterial Potentials of *Blumea Balsamifera l.* Essential Oil Against *Streptococcus Pyogenes and Streptococcus Pneumoniae*: In *Vitro* and In *Silico* Screening

Nguyen T. T. Hai[1], Do T. Q. Huong[2], Nguyen V. Hoang[2], Thanh Q. Bui[1], Phan T. Quy[3], Nguyen V. Phu[4], Nguyen D. Chau[1], Tran Q. Huy[1], Dang T. Hue[2], Nguyen T. A. Nhung[1,*]

[1]*Department of Chemistry, University of Sciences, Hue University, Hue 530000, Vietnam*
[2]*Chi Lang High School, Gia Lai 600000, Vietnam*
[3]*Department of Natural Sciences & Technology, Tay Nguyen University, Buon Ma Thuot, Dak Lak 630000 Vietnam*
[4]*Faculty of Basic Sciences, University of Medicine and Pharmacy, Hue University, Hue 530000, Vietnam*

ARTICLE INFO

Article history:
Received : 24 March 2024
Revised 04 April 2024
Accepted : 03 June 2024
Published online : 01 July 2024

ABSTRACT

Blumea balsamifera L. essential oil (EO) has been known for its diverse antimicrobial activities. This study aimed to determine the antibacterial activity of *Blumea balsamifera* EO against two strains of pathogenic bacteria (*Streptococcus pyogenes* and *Streptococcus pneumoniae*) through *in vitro* and *in silico* methods. The phytochemical screening of the EO and other physicochemical properties (DFT, ADMET, and drug-likeness) were determined using standard protocols. *In vitro* results show that the EO possesses promising antibacterial properties with inhibition zone diameters (IZDs) of 10 ± 2 and 18 ± 2 mm, respectively, for *S. pyogenes* and *S. pneumoniae*; MICs 2.50 and 1.25 µL.mL^{-1}; MBC/MIC ratios 1 and 2. GC-MS characterization of the EO identified 17 constituents (1-17). The binding affinity of the compounds against the target proteins are in the following order: 16-P0C0C7 ($\overline{DS}$ -9.4 kcal.mol^{-1}) > 4-P0C0C7 ($\overline{DS}$ -9.3 kcal.mol^{-1}) > 15-P0C0C7 ≈ 17-P0C0C7 ($\overline{DS}$ -9.2 kcal.mol^{-1}); 3-Q8DQF8 ($\overline{DS}$ -9.0 kcal.mol^{-1}) > 4-Q8DQF8 ($\overline{DS}$ -8.9 kcal.mol^{-1}) > 15-Q8DQF8 ($\overline{DS}$ -8.7 kcal.mol^{-1}); 16-6LU7 ($\overline{DS}$ -9.0 kcal.mol^{-1}) ≈ 17-6LU7 ($\overline{DS}$ -9.1 kcal.mol^{-1}). The phytochemicals potentiality derived from quantum calculation were 3 (3.40 Debye), 15 (2.47 Debye), and 5 (2.03 Debye). The suitability for physicochemical and pharmacokinetic applications was assessed via reference to Lipinski's rule of five and Pires' interpretations, respectively. The analysis shows that (+)-2-Bornanone (3; 58.00 %) was the primary bioactive component responsible for the observable antibacterial activities given by its predominant content and favorable predictions. Compound 3 could further be investigated for its antibacterial activity by isolating and characterizing its pure form.

***Keywords*:** *Blumea balsamifera* L., Antibacterial screening, DFT calculations, GC-MS characterization, molecular docking.

Introduction

The upper respiratory tract is particularly vulnerable to bacterial and viral infections because of its exposure to external aerosols and lack of robust defenses. The most typical impact recently is the COVID-19 pandemic caused by the widespread SARS-CoV-2, which has raised severe public healthcare concerns and is still gaining special attention from the scientific community.[1] The main protease (Mpro) is an important enzyme of the virus, essential for proteolytic maturation of nonstructural proteins[2]; recently, increasing scientific research inputs have reinforced its indispensable role in viral replication.[3] Mpro is implicated as a potential target for antiviral drugs as COVID treatments. The crystalline structure of SARS-CoV-2 main protease was shortly determined after the first breakouts and deposited for public reference onto the RCSB PDB database under the entry 6LU7 (DOI: 10.2210/pdb6LU7/pdb).

*Corresponding author. E mail: ntanhung@hueuni.edu.vn,

Tel: +84986980263

Citation: Hai, NTT, Huong, DTQ, Hoang, NV, Bui, TQ, Quy, PT, Phu, NV, Chau, ND, Huy, TQ, Hue, DT, Nhung, NTA.Antibacterial Potentials of Blumea *Balsamifera* l. Essential Oil Against *Streptococcus Pyogenes* and *Streptococcus Pneumoniae*: in Vitro and In Silico Screening. Trop J Nat Prod Res. 2024; 8(6): 7590 – 7602. https://doi.org/10.26538/tjnpr/v8i6.40

Official Journal of Natural Product Research Group, Faculty of Pharmacy, University of Benin, Benin City, Nigeria

Streptococcus pyogenes is a species of gram-positive, aerotolerant bacteria in the genus *Streptococcus*. It is responsible for acute bacterial pharyngitis, commonly known as strep throat[4]. It is estimated to affect approximately 30 % of children and over 10 % of adults, with approximately 1000 million new cases diagnosed globally per annum, making S. *pyogenes* infection one of the leading healthcare expenses.[5] It is known for a variety of virulence features, including biofilm building, luxS is considered one of the most essential proteins of the bacterium. The importance of luxS has been indirectly proven by various mutagenesis research; the mutation of the luxS gene was observed to alter various virulent activity[6] and pathogenicity.[7] The crystalline structure of S. *pyogenes* luxS protein has been determined experimentally and can be referenced from the UniProtKB database under the entry P0C0C7 (LUXS_STRPY).

Streptococcus pneumoniae is also a gram-positive, spherical bacterium, alpha-hemolytic member of the genus *Streptococcus*. It has been implicated as the major cause of pneumonia worldwide, which is still the primary cause of juvenile death in underdeveloped regions. Evidence shows that *Streptococcus pneumoniae* causes community-acquired pneumonia and meningitis.[8] Like other *Streptococcus* bacteria, luxS is considered one of the most essential proteins of the bacterium. Further, S. *pneumoniae* produces auto-inducers, i.e., Autoinducer-2 (AI-2) assembled by the protein luxS. This family of signaling molecules (AI-2) enhances biofilm formation and motility.[9] The crystalline structure of S. *pneumoniae* luxS protein has also been characterized and deposited onto the UniProtKB database under the entry Q8DQF8 (Q8DQF8_STRR6).

Evidence revealed increased mortality and morbidity when the virus is co-infection with various respiratory bacteria. For instance, 94.2 % of SARS-CoV-2-infected cases (in Jiangsu Province) were also diagnosed in co-infection with other respiratory pathogens (up to 24) within 1-4 days of onset of the first infection.[10] This study also found that *Streptococcus pneumoniae* was the most commonly recorded (along with Klebsiella *pneumoniae*, Haemophilus influenzae, and *Streptococcus pyogenes*). In terms of S. *pneumoniae*-coinfected COVID cases, a medical record reported that all the patients experienced severe respiratory failure and required intensive oxygen supplementation.[11] Therefore, collecting knowledge about the *Streptococcus* bacteria and looking for potential supplemental products are still of necessity, especially those conventionally available for in-house use.

Blumea *balsamifera* is a flowering plant belonging to the genus Blumea of the family Asteraceae. The genus Blumea is widely distributed in Asia's tropical and subtropical regions; Blumea *balsamifera* (L.) is commonly found in Southeast Asia.[12,13] It is described as a soft-hairy and half-woody shrub with a strong aroma and 1-3 m in height. The leaves are simple, alternate, and broadly elongated, with 7-20 cm long toothed margins. The flowers have loose yellow heads scattered along much-branched leafy panicles, including two discoid types: peripheral flowers (tiny and more numerous, with a tubular corolla) and central flowers (large but few, with a campanulate corolla). The fruits are dry, 1-seeded, 10 ribs, and hairy. This species is ruderal, often growing on disturbed land and in grasslands.

Recently, there has been increasing evidence for the medical potential of B. *balsamifera*. In Asian traditional medicine, the herb has long been known as an effective remedy for the common cold, stomach pains, and urolithiasis; it is also used to treat various infected conditions, including open wounds, the urinary tract, and the respiratory system.[14,15] Despite the time-tested folk experiences for its health and medical benefits, the plant has only gained the attention of scientific communities over the past few decades. Regarding the antimicrobial potential, the total plant extracts and essential oil were tested for their antibacterial and antifungal activities[16–18]; the most recent work included the promising properties against S. *pneumoniae*. Regarding compositional characteristics, camphor and limonene are the major active ingredients in the volatile oil extracted from the leaves, yet there were traces of borneol, saponin, sesquiterpene, and tannin.[13,19] Otherwise, to our knowledge, the evidence on the other types of respiratory bacteria is still poorly reported in the literature, and there is still a lack of studies on its composition-activity correlation. Therefore, B. *balsamifera*'s antibacterial potential, especially against respiratory ones, needs further exploration for its bio-chemical availability and antibacterial potentials.

Harnessing the power of computers, in silico research offers significant advantages over traditional experimental methods, i.e., cost-reduction and time-effectiveness. Computer-aided drug design (CADD) helps to identify potential drug candidates quickly and reliably if various computational platforms are exploited appropriately. For example, molecular docking simulation is a cost-effective technique to predict binding mechanisms. Ligand-protein inhibitory potentiality is the perceptual argument based on the physicochemical properties of the potential inhibitors, which can serve as complementary additives for docking-related oversimplification.[20,21] Additionally, quantum chemical computation can contribute to the missing properties, e.g., chemo-physical suitability and intermolecular tendencies. Finally, available pharmacokinetic and pharmacological models can evaluate promising candidates for their appropriateness in drug-development applications. The results can provide a reliable view of the bio-compatible and pharma-suitable potentiality.[22,23]

This study aimed to investigate the antibacterial potentials of B. *balsamifera* essential oil against S. *pyogenes* and S. *pneumoniae* through in vitro and in silico methods.

Materials and Methods

Plant collection, identification, and preparation

Blumea *balsamifera* L. leaves were collected from Chu Phong, Gia Lai province, Vietnam (March 2023). The samples were identified by Dr. Nguyen Thi Thanh Hai and deposited at the University of Sciences, Hue University (voucher no.: DB-02/2023). The harvested leaves were washed with water, dried under, and ground into powder.

Extraction of Essential oil

The essential oil of B. *balsamifera* was obtained by the steam distillation method. The powdered sample (30 kg) was distilled with 50 L of distilled water under reflux. The oil was collected and dried with anhydrous sodium sulfate. The EO obtained was stored in an airtight container until further use.

Microorganisms

S. *pyogenes* (ATCC 19615) and S. *pneumoniae* (ATCC 49619) were supplied by the Microbiology and Parasitology Department, Faculty of Pharmacy, Nguyen Tat Thanh University. The bacteria were cultured in Brain Heart Infusion (BHI) agar, with the addition of defibrinated sheep blood (5 %); condition: temperature 37 °C; duration 24 h. The standardized suspension was prepared by dilution using saline solution (0.85 %) and Tween 80 (0.05 %) until the optical density (OD) value of 0.08-0.12 (at wavelength 625 nm), equivalent to the concentration $1\text{-}2.10^8$ CFU.mL^{-1} was obtained.

In vitro Antibacterial study

B. *balsamifera* essential oil was subjected to antimicrobial tests following the guidelines from The Clinical and Laboratory Standards Institute (CLSI) document M02-A11. In this assay, the Mueller-Hinton agar (MHA) with the addition of defibrinated sheep blood (5 %) was used as the medium in a laboratory petri dish (thickness ca. 4 mm; diameter 90 mm; agar volume ca. 20-25 mL) for each type of bacteria; the bacterial suspension (100 µL) was swabbed evenly onto the agar surface; a circular paper (diameter 6 mm) soaked with an antibacterial sample (5 µL) was placed for the diffusion. The bacteria (i.e., S. *pyogenes* or S. *pneumoniae*) were used in their standardized turbidity. The optical density (OD) values were recorded in the range 0.08-0.12 at λ 625 nm, equivalent to the bacterial concentrations of 1.2×10^8 CFU/mL. The antibiotic candidates (B. *balsamifera* essential oil or the control Ampicillin) were used in their pure forms. Afterward, the dishes were incubated (24 hours; 37 °C; 5 % CO_2) before measuring the inhibition zone diameter (IZD).[24] The procedure was implemented in triplicate to determine the mean IZD, interpreted as follows: 6 mm for no sensitivity or resistance, 7-9 mm for low sensitivity, 10-14 mm for moderate sensitivity, and >14 for high sensitivity, as described by Muanza et al.[25]

Dilution assay

B. *balsamifera* essential oil was subjected to the antimicrobial activity assay following the method of Globus et al.[26] For precursor preparation, the standardized bacterial suspension was diluted 10-fold to yield the turbidity of 10^7 CFU.mL^{-1} before use. The pure essential oil was diluted by Tween 80 (0.05 %) to obtain the initial concentration, followed by a 2-fold serial dilution of the test agent). In this assay, the Mueller-Hinton agar (MHA) with the addition of defibrinated sheep blood (5 %) was used as the medium in each agar-plate well (900 µL) for each bacteria-antibiotics, the antibiotic series (100 µL) was distributed sequentially into the wells (concentrations of 5.0000, 2.5000, 1.2500, 0.6250, 0.3125 and 0.0000 µL.mL^{-1}). The bacterial suspension (1 µL) was dropped on the agar surface, and another plate was used with serial concentrations (0.2500; 0.1250; 0.0625; 0.0312; 0.0156; 0.0000 µL.mL^{-1}) of the control Ampicillin for each bacterial strain. Afterwards, the plates were incubated (24 hours; 37 °C).

Efficacy test

B. *balsamifera* essential oil was subjected to a bactericidal test following the guidelines from The Clinical and Laboratory Standards Institute (CLSI) document M26-A. The MIC-valued and two other MIC-upper bound broths were extracted and subcultured in the Mueller-Hinton agar (MHA) without test agents. Afterwards, the

specimens were incubated (24 hours; 37 °C). The EO minimum bactericidal concentration (MBC) refers to the lowest level of an antimicrobial agent, resulting in microbial death (permanent loss of reproductive capacity).

Spectroscopic characterization

The B. *balsamifera* essential oil was subjected to gas chromatography-mass spectrometry (GC-MS). Instrument: Agilent GC 7890B-MS 5975C, HP-5MS column (30 m × 0.25 mm × 0.25 µm), the carrier gas Helium (13 psi). The GC temperature program: (i) initiating at 70 ^{o}C; (ii) linearly increasing to 280 ^{o}C (10 ^{o}C.min^{-1}). The MS scanning configuration: (i) electron ionization (EI) mode with voltage 70 eV; (ii) range of sector block analyzer from 40 to 400 amu. The sample (1 µL) was split in a ratio of 20:1 before injection. The chemical components detected were identified by reference to the database NIST14. All reagents, solvents, and chemicals were in analytical purity (Sigma-Aldrich, USA).

Computational input preparation

Data from the existing literature and experimental findings were used as the input for the computational screening. In particular, the chemical formulae of potential compounds (1-17) were obtained from GC-MS analysis and drawn using MOE 2022.10, while, the biological assemblies of representative proteins structures were referenced from public protein banks, i.e.: luxS protein of S. *pneumoniae* (UniProtKB: Q8DQF8 (Q8DQF8_STRR6); luxS protein of S. *pyogenes* (UniProtKB: P0C0C7 (LUXS_STRPY)); the main protease of SARS-CoV-2 (PDB: 6LU7 (https://doi.org/10.2210/pdb6LU7/pdb)).

Docking simulation

Molecular docking simulation (by MOE 2022.10 [27]) was done in three steps: (i) Input preparation (configuration: protein active range 4.5 Å, ligand charge-assigning using Gasteiger-Huckel method); (ii) Docking simulation (configuration: retaining poses 10; solutions per iteration 1000; solutions per fragmentation 200); (iii) Re-docking iteration (threshold: root-mean-square deviation (RMSD) values < 2 Å; recommended by MOE).

Quantum calculation

Molecular chemical properties of the investigated structures were given by density functional theory (DFT) calculation using Gaussian 09 without symmetry constraints [28]. Level of theory M052X/6–311++G(d,p) and basis set def2-TZVPP [29] were selected. The converged geometries were checked for the structural global minimum on the potential energy surface (PES) by vibrational frequencies. The frozen-core approximation for non-valence-shell electrons was applied. The resolution-of-identity (RI) approximation was set. The frontier orbital analysis was carried out by NBO 5.1 at the level of theory M052X/def2-TZVPP [30].

Physicochemical properties analysis

Drug-likeness properties of the phytochemicals were predicted by a combinational model. The physical properties parameters were retrieved from QSARIS [31] using the Gasteiger–Marsili method.[32] The references were from Lipinski's rule of five [33], which provides the theoretical criteria for a well membrane-permeable candidate.

ADMET prediction

The pharmacological potentiality of the compounds was also assessed using a combinational model. The parameters were ADMET (absorption, distribution, metabolism, excretion, and toxicity) properties retrieved from SwissADME (Swiss Institute of Bioinformatics; http://www.swissadme.ch/; 30th October 2023). The references were from Pires' theoretical interpretations.[36]

Results and Discussion

The results of the agar diffusion test are shown in Figure 1. The EO of B. *balsamifera* exhibited moderate-to-high inhibitory effects against S. *pyogenes* and S. *pneumoniae*, corresponding to IZDs 10 ± 2 and 18 ± 2 mm, respectively. Meanwhile, the bacteria strains showed high susceptibility to ampicillin, with an IZD of approximately 45 ± 2 mm. This is expected since ampicillin is well-known for treating respiratory tract infections. The dilution-assay results are presented in Figure 2. The results reveal that both S. *pyogenes* and S. *pneumoniae* were effectively inhibited by B. *balsamifera* essential oil at the MICs 2.50 and 1.25 µL.mL^{-1}, respectively. The positive control agent had a MIC value of 1.25 µL.mL^{-1} against both bacterial strains. Similarly, the efficacy trial results are summarized in Table 1. The MBC values of B. *balsamifera* essential oil against S. *pyogenes* and S. *pneumoniae* were 2.50 µL.mL^{-1}, corresponding to MBC/MIC ratios of 1 and 2, respectively. These values lie within the threshold recommended (MBC/MIC ≤ 4) for bactericidal activity.[37]

The potential of B. *balsamifera* essential oil against S. *pyogenes* and S. *pneumoniae* can be preliminarily assessed with an upper-moderate activity, given the in vitro evidence. From the view of in-practice development, natural products are considered more suitable for in-house supplemental products for respiratory infection than commercial antibiotic drugs. From the standpoint of research insight, the plant's bioactivity may be linked to the major components of the total EO, which may also account for its moderate-active candidates.

Phytochemicals in plant extracts have been characterized using different assay methods, including GC-MS. The GC-MS analysis of the EO of B. *balsamifera* revealed 17 components (1-17), as shown in Table 2, and their chemical structures in Figure 3. Particularly, (+)-2-Bornanone (3; 58.00 %) is the predominant compound, followed by Caryophyllene (11; 15.90 %), accounting for the major content of the essential oil. Additionally, 7-epi-Silphiperfol-5-ene (7; 9.01 %), Endo-Borneol (4; 5.82 %), and Silphiperfol-5-ene (6; 3.76 %) are considered to make up the remaining portion. Together, they constitute over 90 % of the volatile parts of the plant. More likely, these constituents might be primarily responsible for the biological activities observed earlier than the minor counterparts. However, any experimental attempts to allocate property-component relationships, including isolation and biological investigation, may be challenging and demanding from a lab-based standpoint.

Molecular docking screening can be used to identify the inhibitory potential of a ligand against a representative protein structure of the host biological subjects, S. *pyogenes*-, S. *pneumoniae*, and SARS-CoV-2-related important enzymes in this work. This should be considered an initial assessment of ligand-protein interaction potentiality rather than a conclusive argument of inhibitory effectiveness. In this scope, the total docking score (DS) values and the number of hydrogen-like bonds are selected as the main indicators for inhibitory effectiveness. They represent pseudo values for Gibbs free energy of ligand-protein complex formation and their strong intermolecular bonds. The primary docking parameters corresponding to the four most vulnerable sites of each protein structure (identified by MOE algorithms) are summarized in Table 3. This regards the interaction of the potential inhibitors (1-17) and the targeted protein structures (P0C0C7, Q8DQF8, and 6LU7). Regarding the luxS representatives, the most effective ligand-protein inhibitory structures against that of S. *pyogenes* were in the following order: 16-P0C0C7 ($\overline{DS}$ -9.4 kcal.mol^{-1}) > 4-P0C0C7 ($\overline{DS}$ -9.3 kcal.mol^{-1}) > 15-P0C0C7 ≈ 17-P0C0C7 ($\overline{DS}$ -9.2 kcal.mol^{-1}). Meanwhile, the corresponding order for that of S. *pneumoniae* is 3-Q8DQF8 ($\overline{DS}$ -9.0 kcal.mol^{-1}) > 4-Q8DQF8 ($\overline{DS}$ -8.9 kcal.mol^{-1}) > 15-Q8DQF8 ($\overline{DS}$ -8.7 kcal.mol^{-1}). These values are not in general considered significantly discrepant and evaluated overall as moderate inhibitory effectiveness, compared to the results found in our previous works on garlic-contained organosulfur phytochemicals (ca. -14 kcal.mol^{-1})[38] and ginger-contained volatile substances (ca. -11 kcal.mol^{-1})[39], which were retrieved from the same docking environment. This is understandable as garlic and ginger generally hold a reputation for robust antibiotic activities amongst folk medication, especially against respiratory bacteria. Coupled with lab-based observations, since there is no

candidate with pronounced potentiality by computer-based predictions, the overall bio-activities of the total essential oil likely correlate to its quantity-predominant constituents rather than to a quality-distinguishing component. Regarding the SARS-CoV-2 representative, the moderate inhibition is also predicted ($\overline{DS}$ from -7 to -9 kcal.mol^{-1}). Particularly, 16-6LU7 ($\overline{DS}$ -9.0 kcal.mol^{-1}) and 17-6LU7 ($\overline{DS}$ -9.1 kcal.mol^{-1}) were assessed as the most stable ligand-protein complex. This only serves as an extended screening in this work without any relation to experimental observables.

The ligand-protein inhibitory configurations for the most stable inhibitory systems regarding each ligand-protein duos are also rendered for visual presentation in Figure 4 (L-P0C0C7), Figure 5 (L-Q8DQF8), and Figure 6 (L-6LU7). First, all the ligands appear to induce good morphological compatibility with the in-site features of the proteins given by the continuous contours in the 2D interaction maps. Also, all the inhibited sites seem to be rather tight cf. the inhibitor sizes. On the positive side, this could promote steric hindrance, thus increasing the inhibitory efficacy. On the other hand, this might deter further structural modification/functionalization to a certain significance. In-detail bonding parameters are summarized in Tables S2 (for ligand-P0C0C7 complexes), S3 (for ligand-Q8DQF8 complexes), and S4 (for ligand-6LU7 complexes) in the supplemental information.

In the scope of quantum calculation, the obtained output gives the preliminary view of the potential inhibitors' bio-medium compatibility and intermolecular interactability given their properties from ab initio insights. This means the argument regards solely the candidates (1-17) without a targeted reference.

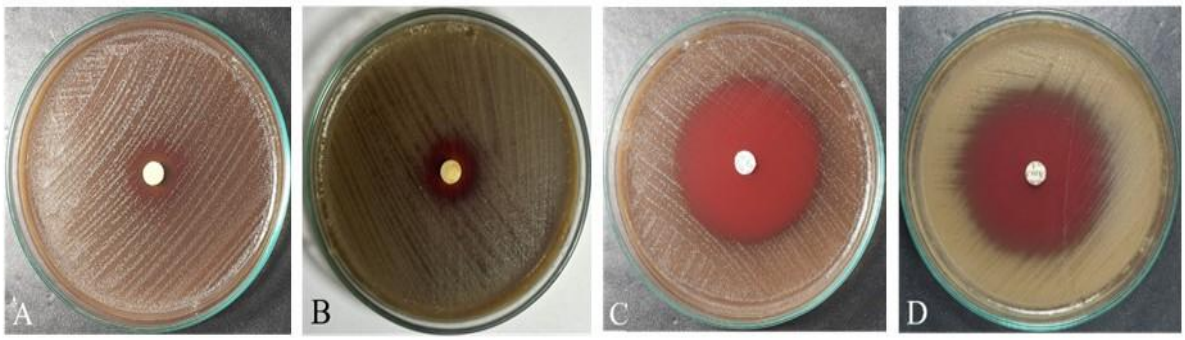

Figure 1: Diffusion-test results: (A) Essential oil - S. *pyogenes*, (B) Essential oil - S. *pneumoniae*, (C) Ampicillin - S. *pyogenes*, (D) Ampicillin - S. *pneumoniae*

Table 1: Identification of bioactive compounds in Blumea *balsamifera* essential oil

Notation	Compound	Formula	Retention time (min)	Percentage (%)
1	β-cis-Ocimene	$C_{10}H_{16}$	4.45	0.11
2	Linalool	$C_{10}H_{18}O$	5.11	0.33
3	(+)-2-Bornanone	$C_{10}H_{16}O$	5.80	58.00
4	Endo-Borneol	$C_{10}H_{18}O$	6.74	5.82
5	(+)-Borneol acetate	$C_{12}H_{20}O_2$	7.41	0.52
6	Silphiperfol-5-ene	$C_{15}H_{24}$	7.94	3.76
7	7-epi-Silphiperfol-5-ene	$C_{15}H_{24}$	8.17	9.01
8	α-Patchoulene	$C_{15}H_{24}$	8.65	0.42
9	Thymohydroquinone dimethyl ether	$C_{12}H_{18}O_2$	8.83	1.21
10	Guaia-6.9-diene	$C_{15}H_{24}$	8.87	0.30
11	Caryophyllene	$C_{15}H_{24}$	9.03	15.90
12	Humulene	$C_{15}H_{24}$	9.41	1.04
13	2-Epi-trans- β -caryophyllene	$C_{15}H_{24}$	9.46	0.89
14	Cadina-1(10).4-diene	$C_{15}H_{24}$	10.03	0.16
15	Caryophyllene oxide	$C_{15}H_{24}O$	10.76	0.56
16	γ-Eudesmol	$C_{15}H_{26}O$	11.29	0.62
17	2-Naphthalenemethanol.1.2.3.4.4a.5.6.8a-octahydro-a.a.4a.8-tetramethyl-(2α .4aα . 8aα)	$C_{15}H_{26}O$	11.54	1.35

Table 2: Results on MBC values Blumea *balsamifera* essential oil

Sample	MBC (µL/mL)		MBC/MIC	
	S. pyogenes	***S. pneumoniae***	***S. pyogenes***	***S. pneumoniae***
Blumea *balsamifera* essential oil	2.5	2.5	1.0	2.0

ISSN 2616-0684 (Print)
ISSN 2616-0692 (Electronic)

Table 3: Screening results on inhibitory potential of 1-17 towards proteins P0C0C7, Q8DQF8., 6LU7 targets

Compound	P0C0C7									Q8DQF8								6LU7								
	Site 1		Site 2		Site 3		Site 4			Site 1		Site 2		Site 3		Site 4			Site 1		Site 2		Site 3		Site 4		
	DS	N	DS	N	DS	N	DS	N	$\overline{DS}$	DS	N	DS	N	DS	N	DS	N	$\overline{DS}$	DS	N	DS	N	DS	N	DS	N	$\overline{DS}$
1	-8.1	1	-7.4	0	-7.3	0	-6.9	0	-7.4	-7.5	0	-7.0	0	-8.0	0	-6.7	0	-7.3	-7.8	0	-7.0	0	-6.8	0	-6.5	0	-7.0
2	-7.2	0	-8.3	1	-7.0	0	-6.8	0	-7.3	-9.2	1	-8.0	0	-7.3	0	-6.9	0	-7.9	-9.3	1	-8.1	0	-7.5	0	-7.0	0	-8.0
3	-7.0	0	-8.7	1	-6.8	0	-6.5	0	-7.3	-9.5	1	-11.0	2	-8.0	0	-7.5	0	-9.0	-9.0	1	-8.0	0	-7.2	0	-6.8	0	-7.8
4	-9.3	1	-12.1	3	-8.0	0	-7.6	0	-9.3	-8.3	0	-8.0	0	-11.5	2	-7.6	0	-8.9	10.8	1	-8.3	0	-7.6	0	-7.2	0	-8.5
5	-8.1	0	-11.4	2	-7.7	0	-7.4	0	-8.7	-8.0	0	-10.9	2	-7.3	0	-6.8	0	-8.3	10.1	1	-8.1	0	-7.4	0	-6.9	0	-8.1
6	-10.3	1	-8.2	0	-7.9	0	-7.5	0	-8.5	-7.0	0	-6.2	0	-9.0	1	-6.3	0	-7.1	-8.6	0	-10.5	1	-7.3	0	-6.6	0	-8.3
7	-10.0	1	-8.3	0	-7.6	0	-7.2	0	-8.3	-6.7	0	-6.5	0	-8.3	0	-7.0	0	-7.1	-8.0	0	-10.3	1	-7.9	0	-7.1	0	-8.3
8	-8.9	1	-7.2	0	-7.0	0	-6.7	0	-7.5	-6.0	0	-6.3	0	-7.9	0	-6.8	0	-6.8	-7.2	0	-8.9	1	-6.7	0	-6.5	0	-7.3
9	-7.8	0	-9.2	1	-6.7	0	-6.3	0	-7.5	-8.8	1	-6.8	0	-7.0	0	-6.1	0	-7.2	-8.7	1	-7.1	0	-6.8	0	-6.1	`0	-7.2
10	-8.7	1	-7.5	0	-7.0	0	-6.6	0	-7.5	-6.6	0	-6.4	0	-7.6	0	-6.0	0	-6.7	-7.3	0	-8.0	0	-6.9	0	-6.4	0	-7.2
11	-10.1	1	-8.3	0	-8.0	0	-7.4	0	-8.5	-7.0	0	-7.2	0	-9.1	1	-6.7	0	-7.5	-8.7	0	-10.0	1	-7.3	0	-7.0	0	-8.3
12	-9.1	1	-7.6	0	-7.2	0	-6.7	0	-7.7	-7.1	0	-6.7	0	-8.2	1	-6.2	0	-7.1	-8.5	1	-7.4	0	-7.1	0	-6.8	0	-7.5
13	-9.5	1	-8.1	0	-7.8	0	-7.3	0	-8.2	-7.1	0	-8.0	0	-7.0	0	-6.5	0	-7.2	-9.8	1	-8.0	0	-7.7	0	-6.7	0	-8.1
14	-9.0	1	-7.8	0	-7.4	0	-7.1	0	-7.8	-6.7	0	-6.4	0	-7.8	0	-6.0	0	-6.7	-8.6	1	-7.5	0	-7.0	0	-6.5	0	-7.4
15	-11.0	2	-9.2	1	-8.8	0	-7.7	0	-9.2	-9.0	1	-11.2	2	-7.6	0	-7.0	0	-8.7	-9.1	1	-10.9	2	-7.6	0	-7.0	0	-8.7
16	-11.2	2	-10.1	1	-8.2	0	-8.0	0	-9.4	10.4	1	-7.9	0	-7.3	0	-6.8	0	-8.1	-9.3	1	-11.1	2	-8.3	0	-7.4	0	-9.0
17	-8.9	0	-11.6	2	-8.4	0	-8.0	0	-9.2	-7.8	0	-7.0	0	-10.8	1	-8.0	0	-8.4	-9.0	1	-11.5	2	-8.4	0	-7.5	0	-9.1

DS: DS value (kcal.mol^{-1}); $\overline{DS}$: Average DS values of different sites (kcal.mol^{-1}); N: Number of hydrophilic interactions

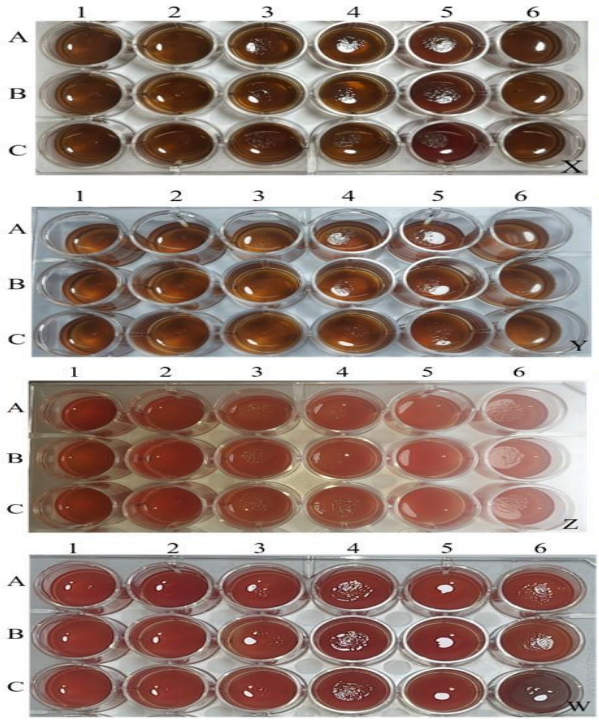

	1	2	3	4	5	6
A	-	-	+	+	+	-
B	-	-	+	+	+	-
C	-	-	+	+	+	-

	1	2	3	4	5	6
A	-	-	-	+	+	-
B	-	-	-	+	+	-
C	-	-	-	+	+	-

	1	2	3	4	5	6
A	-	-	+	+	-	+
B	-	-	+	+	-	+
C	-	-	+	+	-	+

	1	2	3	4	5	6
A	-	-	+	+	-	+
B	-	-	+	+	-	+
C	-	-	+	+	-	+

ISSN 2616-0684 (Print)
ISSN 2616-0692 (Electronic)

Figure 2: Dilution-assay results: (X) Essential oil - S. *pyogenes*, (Y) Essential oil - S. *pneumoniae*, (Z) Ampicillin - S. *pyogenes*, (W) Ampicillin - S. *pneumoniae*; (1-5) assay number, (A-C) assay triplicating; (-) no growth, (+) growth

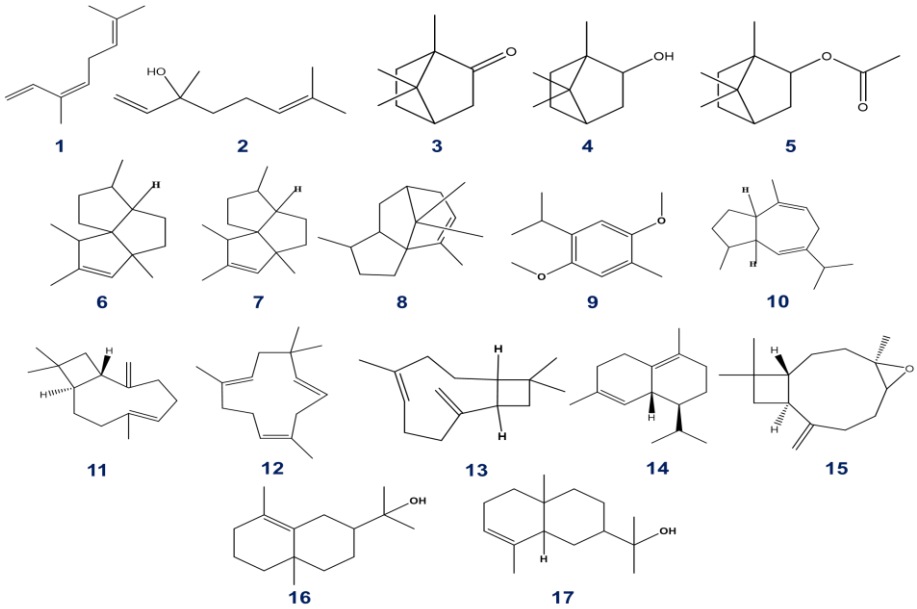

Figure 3: The chemical structures of compounds (1-17) in Blumea *balsamifera* essential oil.

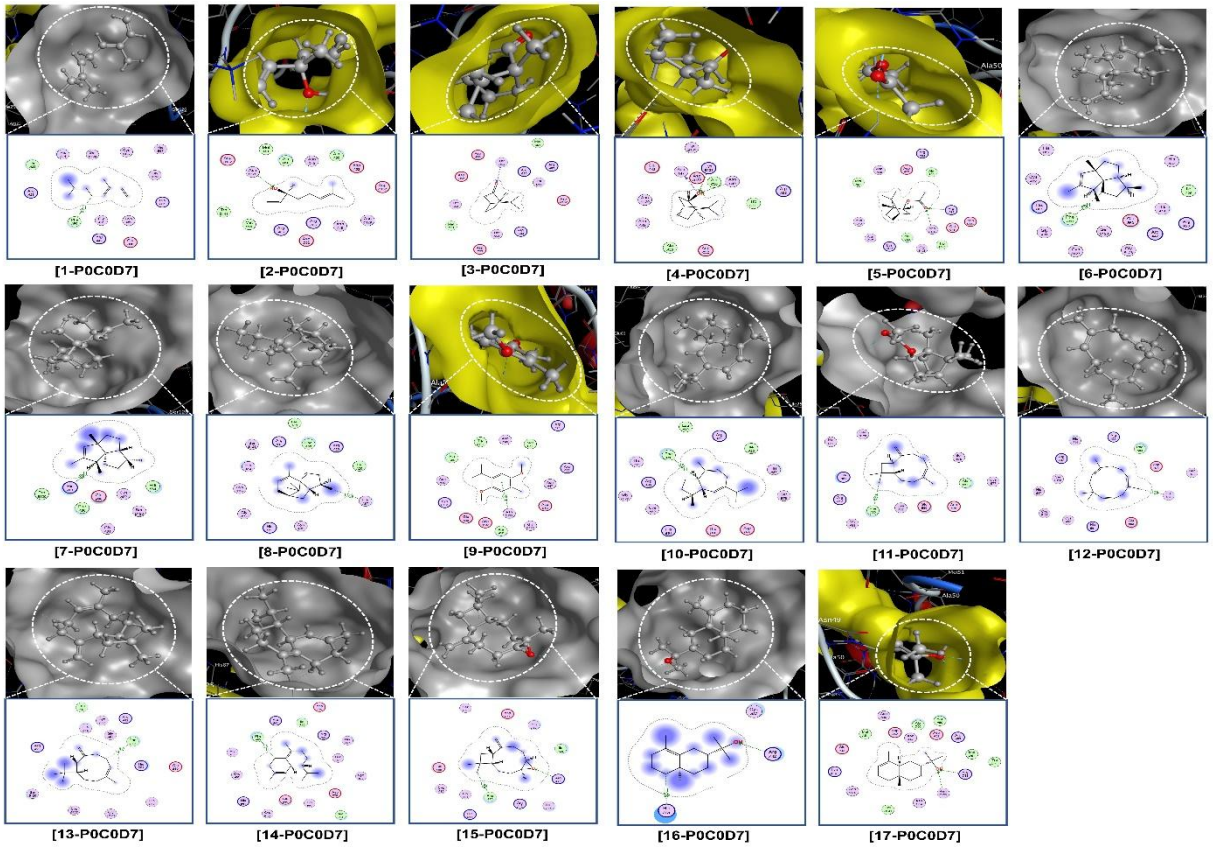

Figure 4: Visual arrangement and interaction map of L-P0C0C7 (L: 1-17) inhibitory structures; dashed arrow: hydrogen-like bonding, blurry purple: van der Waals interaction, dashed contour: conformational fitness

The geometry-optimized structures are presented in Figure 7. Overall, without any geometrical constraints or abnormal bonding parameters (i.e., angles and length), the input structures can self-consistently converge easily during the computational iterations. This, to some degree, verifies the source of the compounds, which are often known to exist stably in nature. The characteristic ground state energy and dipole moment are given in Table 4. The former measures the energetic stability of a structure, thus negatively correlating to its chemical activeness; the latter provides information on its dipole-dipole interacting potential. Firstly, the more stable a molecule is, the

more favoured it should be for inhibitory application. It is likely to retain the chemical structures and properties before reaching its biological targets, thus making it possible to maintain its biological activities. All the compounds register low-negative energy without noticeable differences (avg. -550 a.u.). In particular, 1 (-390.69 a.u.) is the least stable component, thus most likely to induce chemical reactions with the physicochemical constituents, while the major components, i.e., 3, 4, 6, 11, register upper-bound values (from 460 to 586 a.u.), thus predicted with high chemical inertia. Secondly, a higher dipole-moment value means the host molecule would be more compatible with a dipole-solvent environment, such as physicochemical media. This leads to an upheld evaluation for 3 (3.40 Debye), 15 (2.47 Debye), and 5 (2.03 Debye); the foremost candidate is also composed of more than half of B. *balsamifera* essential oil. In addition, 4 (1.62 Debye) is still considerable, while 6 and 11 (under 0.5 Debye) are of low desirability. The distributions of molecular electrostatic potential (MEP) are visualized in Figure 8. In principle, the configuration is based on the electronic density of different regions on the molecular plane; therefore, this can be utilized for perceptual arguments on its flexibility when in inhibitory contact with external structures, especially those with arbitrary or irregular surface features. All the molecules seem to condense their electron distribution into the main functionals (e.g., oxygen- and nitrogen-based groups). In other words, in an inhibitory formation, they are expected to rely solely on either these main groups (for hydrophilic bonding) or van der Waals interactions (for hydrophobic bonding). This is consistent with the predictions from the docking-based platform.

Table 4: Ground state electronic energy and dipole moment values of 1-17

Compound	Ground state electronic energy (a.u.)	Dipole moment (Debye)
1	-390.69	0.73
2	-467.15	1.93
3	-465.10	3.40
4	-467.20	1.62
5	-619.89	2.02
6	-586.14	0.29
7	-586.14	0.29
8	-586.13	0.24
9	-618.63	0.13
10	-586.10	0.24
11	-586.07	0.39
12	-586.07	0.46
13	-586.07	0.39
14	-586.12	0.31
15	-661.30	2.47
16	-662.59	1.67
17	-662.59	1.56

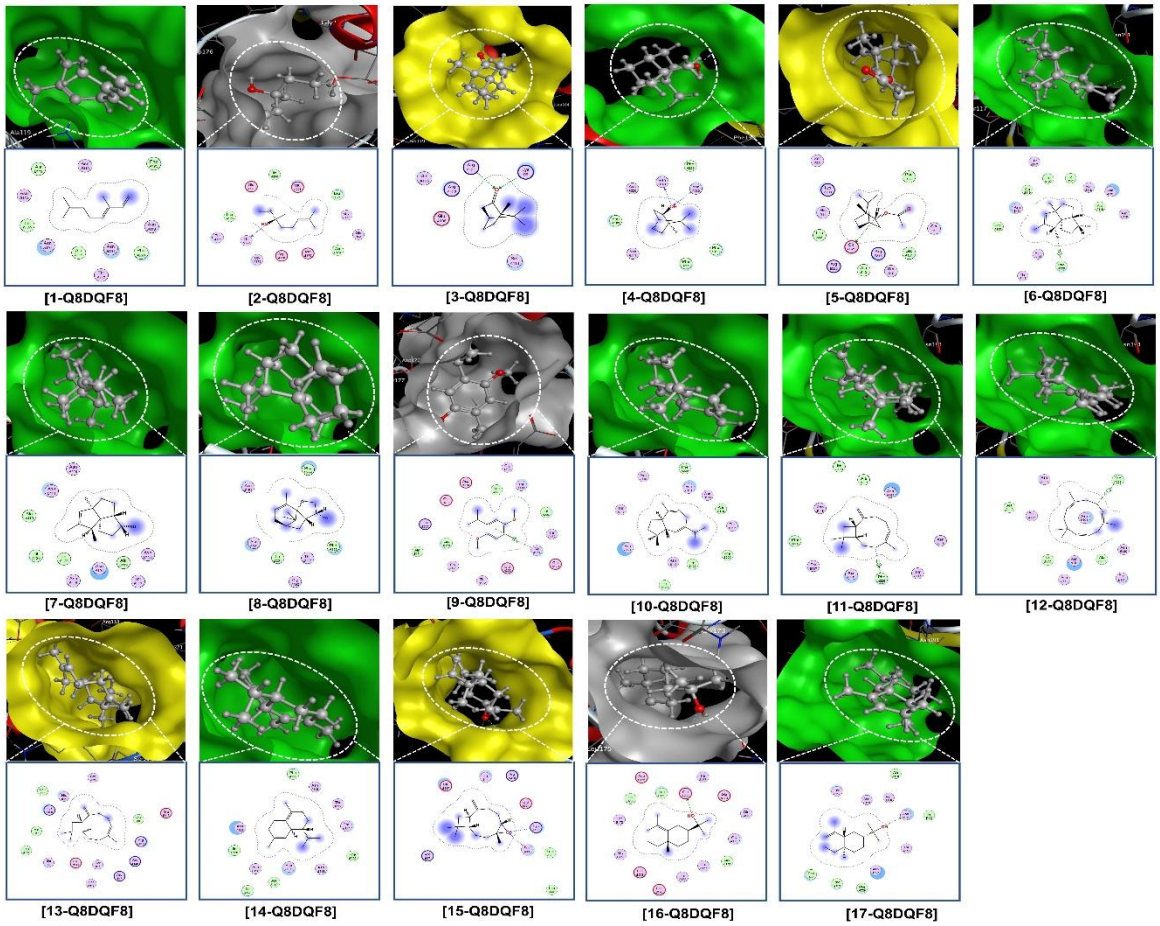

Figure 5: Visual arrangement and interaction map of L-Q8DQF8 (L: 1-17) inhibitory structures; dashed arrow: hydrogen-like bonding, blurry purple: van der Waals interaction, dashed contour: conformational fitness

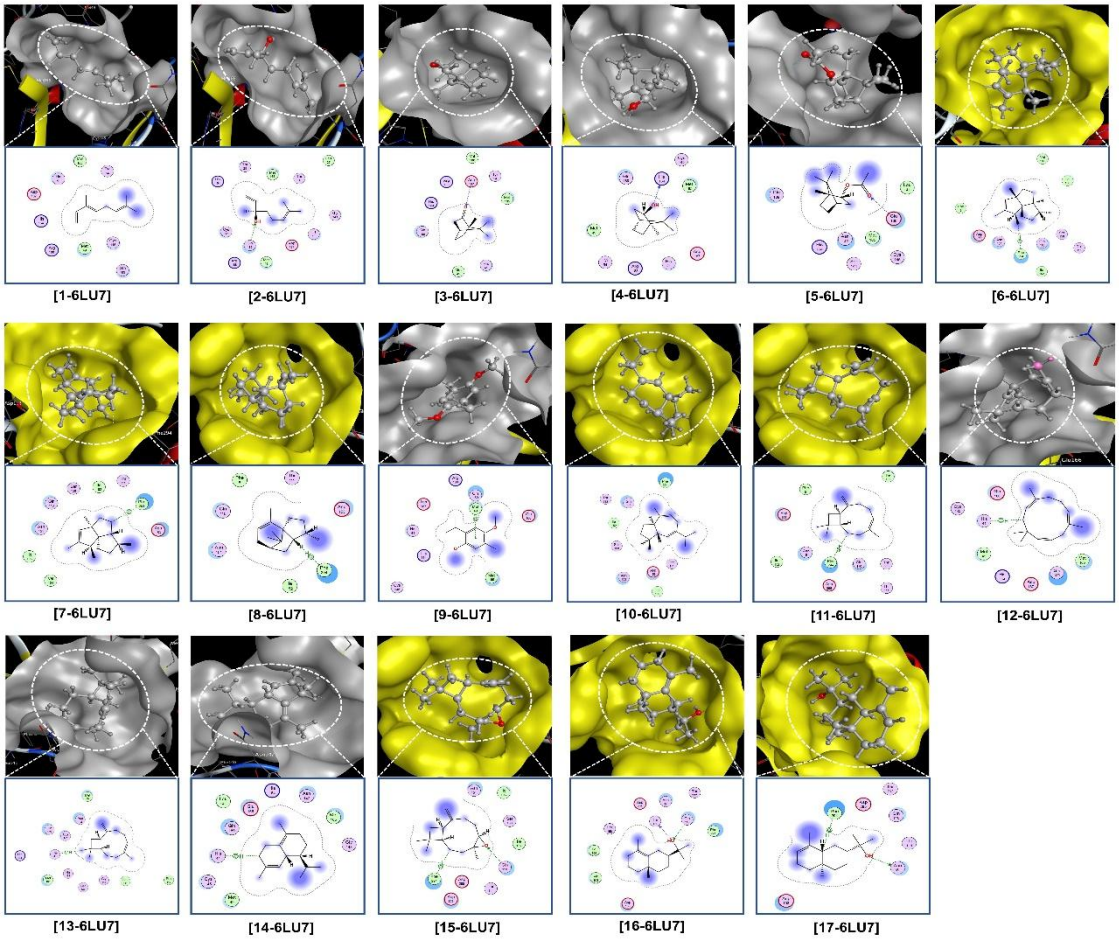

Figure 6: Visual arrangement and interaction map of L-6LU7 (L: 1-17) inhibitory structures; dashed arrow: hydrogen-like bonding, blurry purple: van der Waals interaction, dashed contour: conformational fitness

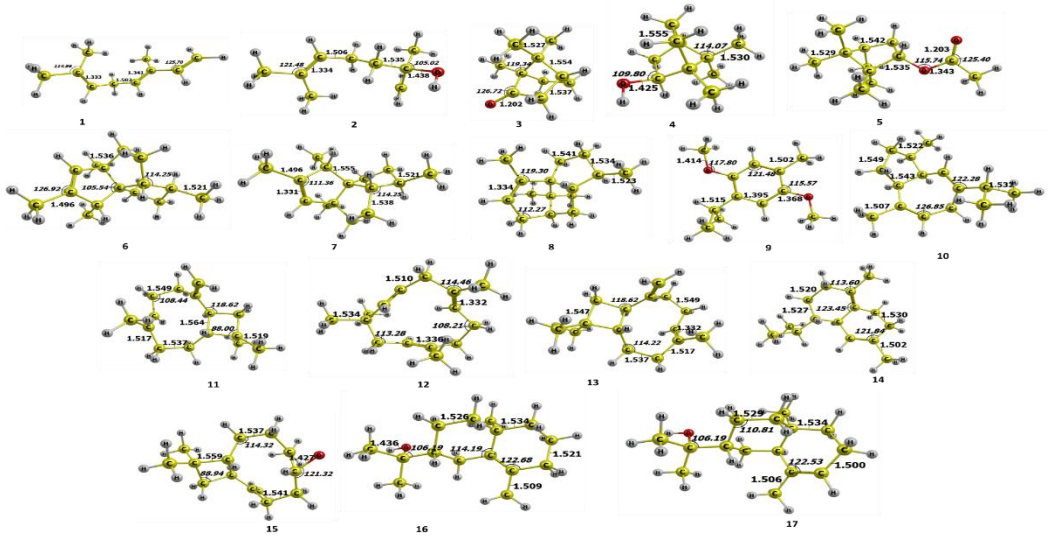

Figure 7: Geometrically optimal structures of 1-17 in Blumea *balsamifera* essential oil; length (Å), angle (°)

The physical properties of the compounds are summarized in Table 5. These include molecular mass (Da), polarizability (Å^3), size (Å), and dispersion coefficients (logP and logS), retrieved from the QSARIS system; maximum number of hydrogen bonds, counted from docking results. All the compounds are considered to satisfy the drug-like assessments based on Lipinski's criteria, i.e., molecular mass < 230 amu; hydrogen-like donors < 5; hydrogen-like acceptors < 5; partition coefficient logP < +5. Besides, the highest size (415.3 Å) of 12 might signify that it is slightly more under spatial constraints, cf. others. Also, there were no pronounced differences in their polarizability. The

lowest value (18.6 Å) of 3 suggests it is less likely to be polarly induced than others. This property reflects the sensitivity of a structure to external electric fields such as those created by other polarized agents (amino-acid-based protein structures); the unit conversion is given by Claussius-Mossotti relation: $10^6/4\pi\epsilon_0\ [\mathrm{A}^2.\mathrm{s}^4.\mathrm{kg}^{-1}] \equiv 1\ [\mathrm{cm}^3]$ [40]. The analysis shows that B. *balsamifera* essential oil is highly compatible with physicochemical environments.

The ADMET properties are summarized in Table 6. These include absorption, distribution, metabolism, excretion, and toxicity. The ADMET results indicate that there were no profound concerns about the compounds when in consideration of Pires' interpretations. Regarding absorption, they showed good compatibility via oral intake: high intestinal absorption (over 90 %); low Caco2 permeability (log Papp < 2×10^{-8}); no interaction with the P-glycoprotein family. Regarding distribution, they are predicted to accumulate in tissue (logVDss > 0.45), readily cross the blood-brain barrier (logBB < -1), and partially penetrate the central nervous system (-3 < logPS < -2). Regarding metabolism, they showed no significant effects on the activities of the cytochromes P450 family. With respect to excretion, the compounds are unlikely to be excreted by organic cation transporter 2, thus conducive to prolonged circulation in the body and retaining medicinal effects for a long duration. In terms of toxicity, the safety for medical use is previsedconcerning all candidates, i.e., the compounds have no mutagenic potentials; no potential for fatal ventricular arrhythmia as hERG inhibitors; no hepatotoxicity; certain skin sensitization; marked toxicity to bacterium T. *Pyriformis* (pIGC50 >> -0.5) yet particular safety to animal organisms, e.g., fish Fathead Minnows (logLC50 >> -0.3). Therefore, B. *balsamifera* essential oil is favourable for further development for pharmaceutical applications.

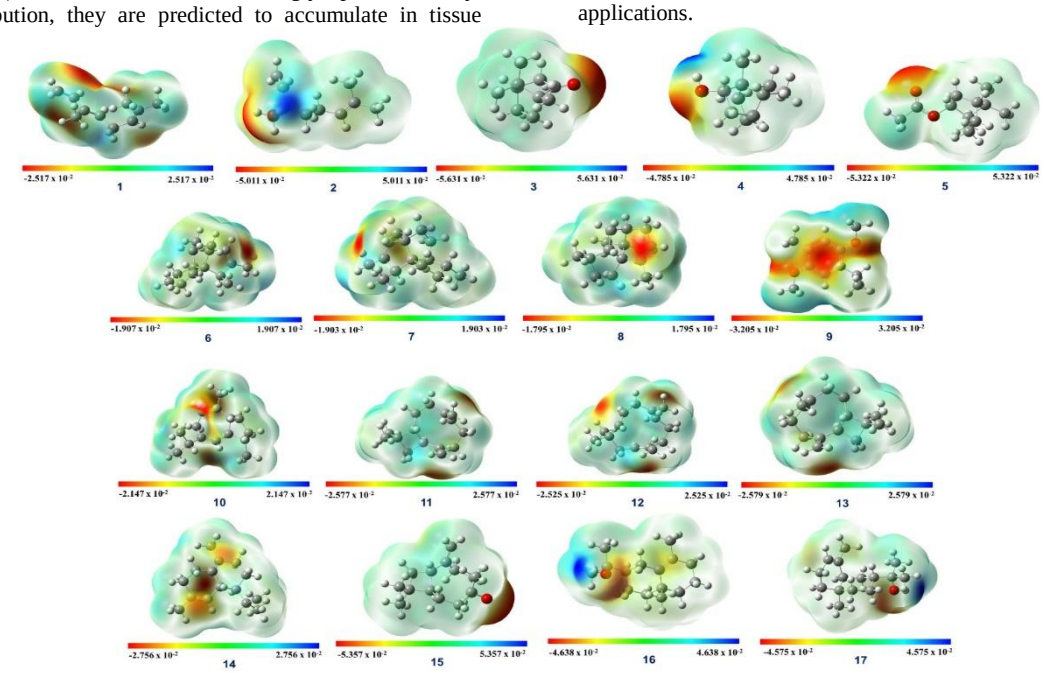

Figure 8: Molecular electrostatic potential (MEP) map of 1-17; reddish region: negative electrostatic potential, bluish region: positive electrostatic potential, greenish region: null electrostatic potential

Table 5: Physicochemical properties of studied compounds 1-17

Ligand	Volume (Å)	Mass (amu)	Polarisability ($Å^3$)	Dispersion cefficients		Hydrogen-bond counts (P0C0C7/Q8DQF8/6LU7)
				logP	logS	
1	293.5	136.4	19.7	4.13	-3.78	1/0/1
2	297.9	154.3	19.3	2.17	-2.02	1/1/1
3	262.3	152.4	18.6	1.93	-2.09	1/2/1
4	260.3	154.5	19.2	2.51	-2.19	3/2/1
5	323.9	196.3	20.8	3.10	-2.81	2/2/1
6	359.7	204.5	25.6	4.45	-4.36	1/1/1
7	362.5	204.4	26.1	4.24	-4.03	1/0/1
8	360.8	204.5	25.0	4.45	-4.51	1/0/1
9	341.2	194.4	24.3	3.32	-2.87	1/1/1
10	387.8	204.3	25.1	4.68	-4.79	1/0/0
11	380.6	204.4	26.8	4.78	-4.35	1/1/1
12	415.3	204.5	27.6	4.49	-3.91	1/1/1
13	398.7	204.4	26.2	4.96	-4.75	1/0/1
14	382.1	204.3	25.9	4.75	-3.71	1/0/1
15	378.3	220.4	26.8	3.66	-4.23	2/2/2
16	385.5	222.5	27.5	3.02	-3.61	2/1/2

17	376.4	222.6	26.4	3.22	-3.83	2/1/2

Table 6: ADMET-based pharmacokinetics and pharmacology of the studied compounds 1-17

Properties	Units	1	2	3	4	5	6	7	8
Absorption									
Water solubility	(1)	-4.446	-2.612	-2.895	-2.462	-3.03	-5.964	-5.964	-5.847
Caco2 permeability	(2)	1.406	1.493	1.499	1.484	1.855	1.397	1.397	1.394
Intestinal absorption (human)	(3)	94.726	93.163	95.965	93.439	95.366	95.564	95.564	94.515
Skin Permeability	(4)	-1.065	-1.737	-2.002	-2.174	-2.233	-1.934	-1.934	-1.833
P-glycoprotein substrate	(5)	No	No	No	No	No	No	No	No
P-glycoprotein I inhibitor	(5)	No	No	No	No	No	No	No	No
P-glycoprotein II inhibitor	(5)	No	No	No	No	No	No	No	No
Distribution									
VDss (human)	(6)	0.336	0.152	0.331	0.337	0.307	0.732	0.732	0.751
Fraction unbound (human)	(6)	0.387	0.484	0.459	0.486	0.412	0.124	0.124	0.157
BBB permeability	(7)	0.761	0.598	0.612	0.646	0.553	0.829	0.829	0.818
CNS permeability	(8)	-1.848	-2.339	-2.158	-2.331	-2.399	-1.625	-1.625	-1.759
Metabolism									
CYP2D6 substrate	(5)	No	No	No	No	No	No	No	No
CYP3A4 substrate	(5)	No	No	No	No	No	Yes	Yes	Yes
CYP1A2 inhibitor	(5)	No	No	No	No	No	Yes	Yes	No
CYP2C19 inhibitor	(5)	No	No	No	No	No	No	No	No
CYP2C9 inhibitor	(5)	No	No	No	No	No	No	No	No
CYP2D6 inhibitor	(5)	No	No	No	No	No	No	No	No
CYP3A4 inhibitor	(5)	No	No	No	No	No	No	No	No
Excretion									
Total Clearance	(9)	0.441	0.446	0.109	1.035	1.029	0.994	0.994	0.973
Renal OCT2 substrate	(5)	No	No	No	No	No	No	No	No
Toxicity									
AMES toxicity	(5)	No	No	No	No	No	No	No	No
Max. tolerated dose (human)	(10)	0.636	0.774	0.473	0.577	0.526	-0.225	-0.225	-0.142
hERG I inhibitor	(5)	No	No	No	No	No	No	No	No
hERG II inhibitor	(5)	No	No	No	No	No	No	No	No
Oral Rat Acute Toxicity (LD50)	(11)	1.636	1.704	1.653	1.707	1.904	1.581	1.581	1.552
Oral Rat Chronic Toxicity (LOAEL)	(12)	2.427	2.024	1.981	1.877	1.875	1.372	1.372	1.334
Hepatotoxicity	(5)	No	No	No	No	No	No	No	No
Skin Sensitization	(5)	No	Yes	Yes	Yes	Yes	No	No	No
T. *pyriformis* toxicity	(13)	0.792	0.515	0.233	0.175	0.557	1.45	1.45	1.431
Minnow toxicity	(14)	0.784	1.277	1.458	1.727	1.593	0.246	0.246	0.452

Table 6. (continued)

Properties	Units	9	10	11	12	13	14	15	16	17
Absorption										
Water solubility	(1)	-3.158	-6.208	-5.555	-5.191	-5.555	-5.915	-4.321	-4.518	-4.422
Caco-2 permeability	(2)	1.656	1.433	1.423	1.421	1.423	1.422	1.414	1.495	1.501
Intestinal absorption (human)	(3)	95.164	96.457	94.845	94.682	94.845	96.128	95.669	92.234	93.022
Skin Permeability	(4)	-1.581	-1.544	-1.58	-1.739	-1.58	-1.462	-3.061	-1.85	-1.874
P-glycoprotein substrate	(5)	No	No	No	Yes	No	No	No	No	No
P-glycoprotein I inhibitor	(5)	No	No	No	No	No	No	No	No	No

P-glycoprotein II inhibitor	(5)	No	No	No	No	No	No	No	No	No
Distribution										
VDss (human)	(6)	0.378	0.67	0.652	0.505	0.652	0.689	0.564	0.487	0.486
Fraction unbound (human)	(6)	0.172	0.122	0.263	0.347	0.263	0.196	0.327	0.273	0.276
BBB permeability	(7)	0.317	0.81	0.733	0.663	0.733	0.773	0.647	0.581	0.594
CNS permeability	(8)	-1.809	-1.641	-2.172	-2.555	-2.172	-1.945	-2.521	-2.299	-2.309
Metabolism										
CYP2D6 substrate	(5)	No	No	No	No	No	No	No	No	No
CYP3A4 substrate	(5)	No	No	No	No	No	No	No	No	No
CYP1A2 inhibitor	(5)	Yes	No	No	No	No	No	Yes	No	No
CYP2C19 inhibitor	(5)	No	No	No	No	No	No	Yes	Yes	Yes
CYP2C9 inhibitor	(5)	No	No	No	No	No	No	Yes	Yes	No
CYP2D6 inhibitor	(5)	No	No	No	No	No	No	No	No	No
CYP3A4 inhibitor	(5)	No	No	No	No	No	No	No	No	No
Excretion										
Total Clearance	(9)	0.352	1.188	1.088	1.282	1.088	1.182	0.905	1.027	1.03
Renal OCT2 substrate	(5)	No	No	No	No	No	No	No	No	No
Toxicity										
AMES toxicity	(5)	No	No	No	No	No	No	No	No	No
Max. tolerated dose (human)	(10)	0.931	0.115	0.351	0.551	0.351	0.213	0.148	0.055	0.131
hERG I inhibitor	(5)	No	No	No	No	No	No	No	No	No
hERG II inhibitor	(5)	No	No	No	No	No	No	No	No	No
Oral Rat Acute Toxicity (LD50)	(11)	1.846	1.557	1.617	1.766	1.617	1.552	1.548	1.681	1.68
Oral Rat Chronic Toxicity (LOAEL)	(12)	2.248	1.497	1.416	1.336	1.416	1.448	1.224	1.249	1.231
Hepatotoxicity	(5)	No	No	No	No	No	No	No	No	No
Skin Sensitization	(5)	Yes	Yes	Yes	Yes	Yes	Yes	Yes	Yes	Yes
T. *pyriformis* toxicity	(13)	1.384	1.728	1.401	1.451	1.401	1.61	1.079	1.524	1.522
Minnow toxicity	(14)	0.387	-0.022	0.504	0.716	0.504	0.093	0.955	0.842	0.819

Conclusion

This study establishes the preliminary correlation between B. *balsamifera*'s EO components and potential antibacterial activities, particularly against S. *pyogenes* and S. *pneumoniae*. Various in vitro tests on the essential oil showed upper-intermediate antibacterial properties (IZDs 10 ± 2 and 18 ± 2 mm; MICs 2.50 and 1.25 µL.mL^{-1}; MBC/MIC ratios 1 and 2). GC-MS identified 17 (1-17), with (+)-2-Bornanone (3; 58.00 %), Caryophyllene (11; 15.90 %), 7-epi-Silphiperfol-5-ene (7; 9.01 %), Endo-Borneol (4; 5.82 %), and Silphiperfol-5-ene (6; 3.76 %) as the major constituents. Docking simulation predicts moderate inhibitory effectiveness, with 16-P0C0C7 having the highest docking score of 9.4 kcal.mol^{-1}). Quantum calculation favoured 3 (3.40 Debye), 15 (2.47 Debye), and 5 (2.03 Debye) physicochemical compatibility, further confirmed by physicochemical and pharmacokinetic analyses for suitability for biological and pharmacological developments. The study concludes that (+)-2-Bornanone (3) is the primary bioactive component responsible for the observable antibacterial activities. This compound can further be investigated for its biological through isolation, in vitro or in vivo.

Conflict of Interest

The authors declare no conflict of interest.

Authors' Declaration

The authors hereby declare that the work presented in this article is original and that any liability for claims relating to the content of this article will be borne by them.

Acknowledgments

Nguyen Thi Ai Nhung acknowledges the partial support from Hue University under the Core Research Program [Project No. NCTB.DHH.2024.04]. This research was conducted at the Institute of Applied Research in Science and Technology, University of Sciences, Hue University.

References

1. Hu B, Guo H, Zhou P, Shi ZL. Characteristics of SARS-CoV-2 and COVID-19. Nat Rev Microbiol. 2021;19(3):141–54.
2. Li X, Song Y. Structure and function of SARS-CoV and SARS-CoV-2 main proteases and their inhibition: A comprehensive review. Eur J Med Chem. 2023;115772.
3. Hu Q, Xiong Y, Zhu G, Zhang Y, Zhang Y, Huang P, Ge G. The SARS CoV 2 main protease (Mpro): structure, function, and emerging therapies for COVID 19. MedComm. 2022;3(3):e151.
4. Shulman ST, Bisno AL, Clegg HW, Gerber MA, Kaplan EL, Lee G, Martin JM, Van Beneden C. Clinical practice guideline for the diagnosis and management of group A

streptococcal pharyngitis: 2012 update by the Infectious Diseases Society of America. Clin Infect Dis. 2012;55(10):e86–102.
5. Avire NJ, Whiley H, Ross K. A Review of *Streptococcus pyogenes*: Public health risk factors, prevention and control. Pathogens. 2021;10(2):Article ID 248.
6. Lyon WR, Madden JC, Levin JC, Stein JL, Caparon MG. Mutation of luxS affects growth and virulence factor expression in *Streptococcus pyogenes*. Mol Microbiol. 2001;42(1):145–57.
7. Kang SO, Caparon MG, Cho KH. Virulence gene regulation by CvfA, a putative RNase: the CvfA-enolase complex in *Streptococcus pyogenes* links nutritional stress, growth-phase control, and virulence gene expression. Infect Immun. 2010;78(6):2754–67.
8. Van de Beek D, de Gans J, Tunkel AR, Wijdicks EFM. Community-acquired bacterial meningitis in adults. N Engl J Med. 2006;354(1):44–53.
9. Song S, Wood TK. The primary physiological roles of autoinducer 2 in *Escherichia coli* are chemotaxis and biofilm formation. Microorganisms. 2021;9(2):386.
10. Zhu X, Ge Y, Wu T, Zhao K, Chen Y, Wu B, Zhu F, Zhu B, Cui L. Co-infection with respiratory pathogens among COVID-2019 cases. Virus Res. 2020;285:ID 198005.
11. Pal C, Przydzial P, Chika-Nwosuh O, Shah S, Patel P, Madan N. *Streptococcus pneumoniae* coinfection in COVID-19: a series of three cases. Case Rep Pulmonol. 2020; ID 8849068.
12. Peng Y, Yang C, Luo Y. *Blumea htamanthii* (Asteraceae), a new species from Myanmar. PhytoKeys. 2020;138:225.
13. Pang Y, Wang D, Fan Z, Chen X, Yu F, Hu X, Wang K, Yuan L. *Blumea balsamifera* - A phytochemical and pharmacological review. Molecules. 2014;19(7):9453–77.
14. Chu SS, Du SS, Liu ZL. Fumigant compounds from the essential oil of Chinese *Blumea balsamifera* leaves against the maize weevil (*Sitophilus zeamais*). J Chem. 2013;1–7.
15. Bhuiyan MNI, Chowdhury JU, Begum J. Chemical components in volatile oil from *Blumea balsamifera* (L.) DC. Bangladesh J Bot. 2009;38(1):107–9.
16. Sakee U, Maneerat S, Cushnie TPT, De-Eknamkul W. Antimicrobial activity of *Blumea balsamifera* (Lin.) DC. extracts and essential oil. Nat Prod Res. 2011;25(19):1849–56.
17. Ismail NA, Matawali A, Kanak FA, Lee PC, How SE, Goh LPW, Gansau JA. Antimicrobial activities and phytochemical properties of *Blumea balsamifera* against pathogenic microorganisms. J Med Life. 2022;15(8):951.
18. Yang H, Gao Y, Long L, Cai Y, Liao J, Peng J, Wang L. Antibacterial effect of *Blumea balsamifera* (L.) DC. essential oil against *Staphylococcus aureus*. Arch Microbiol. 2021;203(7):3981–8.
19. Hanh TTH, Giang VH, Trung NQ, Van Thanh N, Quang TH, Cuong NX. Chemical constituents of *Blumea balsamifera*. Phytochem Lett. 2021;43:35–9.
20. Thao TTP, Bui TQ, Quy PT, Bao NC, Van Loc T, Van Chien T, Chi NL, Van Tuan N, Van Sung T, Nhung NTA. Isolation, semi-synthesis, docking-based prediction, and bioassay-based activity of Dolichandrone spathacea iridoids: new catalpol derivatives as glucosidase inhibitors. RSC Adv. 2021;11:11959–75.
21. Thao TTP, Bui TQ, Hai NTT, Huynh LK, Quy PT, Bao NC, Dung NT, Chi NL, Van Loc T, Smirnova IE. Newly synthesised oxime and lactone derivatives from Dipterocarpus alatus dipterocarpol as anti-diabetic inhibitors: experimental bioassay-based evidence and theoretical computation-based prediction. RSC Adv. 2021;11(57):35765–82.
22. Quy PT, Bui TQ, Bon N V, Phung PTK, Duc DPN, Nhan DT, Phu N V, To DC, Nhung NTA. Euonymus laxiflorus Champ. bioactive compounds inhibited α-glucosidase and protein phosphatase 1B – A computational approach towards the discovery of antidiabetic drugs. Trop J Nat Prod Res. 2023;7(5):2974–91.
23. Nguyen NPD, Quy PT, To DC, Bui TQ, Phu N V., My TTA, Nguyen PH, Kien NH, Hai NTT, Nhung NTA. Combinatory in silico study on anti-diabetic potential of Ganoderma lucidum compounds against α-glucosidase. Trop J Nat Prod Res. 2023;7(7):3421–32.
24. Castilho AL, Caleffi-Ferracioli KR, Canezin PH, Siqueira VLD, de Lima Scodro RB, Cardoso RF. Detection of drug susceptibility in rapidly growing mycobacteria by resazurin broth microdilution assay. J Microbiol Methods. 2015;111:119–21.
25. Muanza DN, Kim BW, Euler KL, Williams L. Antibacterial and antifungal activities of nine medicinal plants from Zaire. Int J Pharmacogn. 1994;32(4):337–45.
26. Golus J, Sawicki R, Widelski J, Ginalska G. The agar microdilution method–a new method for antimicrobial susceptibility testing for essential oils and plant extracts. J Appl Microbiol. 2016;121(5):1291–9.
27. Molecular Operating Environment (MOE), 2022.02 Chemical Computing Group ULC, 910-1010 Sherbrooke St. W., Montreal, QC H3A 2R7, Canada, 2024.
28. Gaussian 09, Revision A.02, M. J. Frisch, G. W. Trucks, H. B. Schlegel, G. E. Scuseria, M. A. Robb, J. R. Cheeseman, G. Scalmani, V. Barone, G. A. Petersson, H. Nakatsuji, X. Li, M. Caricato, A. Marenich, J. Bloino, B. G. Janesko, R. Gomperts, B. Mennucci.
29. Zhao Y, Schultz NE, Truhlar DG. Design of density functionals by combining the method of constraint satisfaction with parametrization for thermochemistry, thermochemical kinetics, and noncovalent interactions. J Chem Theory Comput. 2006;2(2):364–82.
30. Reed AE, Weinstock RB, Weinhold F. Natural population analysis. J Chem Phys. 1985;83(2):735–46.
31. Cameron DR. Computer software reviews. J Am Chem Soc. 2001;123(35):8644–8645.
32. Gasteiger J, Marsili M. Iterative partial equalization of orbital electronegativity-a rapid access to atomic charges. Tetrahedron. 1980;36(22):3219–28.
33. Lipinski CA, Lombardo F, Dominy BW, Feeney PJ. Experimental and computational approaches to estimate solubility and permeability in drug discovery and development settings. Adv Drug Deliv Rev. 1997;23:3–25.
34. Ahsan MJ, Samy JG, Khalilullah H, Nomani MS, Saraswat P, Gaur R, Singh A. Molecular properties prediction and synthesis of novel 1,3,4-oxadiazole analogues as potent antimicrobial and antitubercular agents. Bioorganic Med Chem Lett. 2011;21(24):7246–50.
35. Mazumdera J, Chakraborty R, Sena S, Vadrab S, Dec B, Ravi TK. Synthesis and biological evaluation of some novel quinoxalinyl triazole derivatives. Der Pharma Chem. 2009;1(2):188–98.
36. Pires DEV, Blundell TL, Ascher DB. pkCSM: Predicting small-molecule pharmacokinetic and toxicity properties using graph-based signatures. J Med Chem. 2015;58(9):4066–72.
37. CLSI. Performance Standards for Antimicrobial susceptibility Testing, 30th Edition. CLSI Doc M100. 2020;
38. Thai NM, Bui TQ, Quy PT, Thanh Hai NT, To DC, Quang DT, Co NQ, Triet NT, Ai Thuan NT, To Nhi NT, Tham VM, Ai Nhung NT. Potentiality of organosulfur compounds against SARS-CoV-2-coinfected bacteria S *pyogenes* and S *pneumoniae*: A cross-platform analysis from computational chemistry. Nat Prod Commun. 2023;18(8):1–23.
39. Van Hue N, Cuong TD, Quy PT, Bui TQ, Hai NTT, Triet NT, Thanh DD, Nhi NTT, Thai NM, Van Chen T, Nhung NTA. Antimicrobial properties of Distichochlamys citrea M.F. Newman rhizome n-hexane extract against *Streptococcus pyogenes*: experimental evidences and computational screening. ChemistrySelect. 2022;7(17).

ISSN 2616-0684 (Print)
ISSN 2616-0692 (Electronic)

40. Feynman R. The Feynman lectures on physics - Volume II. Millenium. Gottlieb MA, editor. New York: Basic Books; 2010. 11.3.